

it increases, until it reaches, near the cutoff, a value that is generally comparable to its value at zero frequency, with opposite sign. Furthermore, in this example, the length correction is far from negligible, varying in absolute value from 0 to a quarter of the radius a .

It may be noted that the solid curve is not drawn until the cutoff frequency. This is because the procedure of calculation of the length correction [Eqs. (9) and (10)] fails as soon as the higher order modes, although still evanescent, can no longer be considered as a small perturbation.

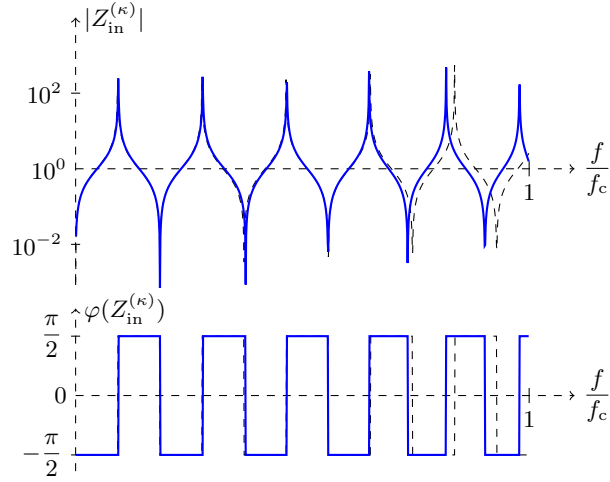
When varying the curvature of the bent portion, while keeping constant the lengths l_u , l_b and l_d , the evolution with frequency of length correction is roughly the same, with mainly the overall amplitude of the curve changing: the larger the curvature, the larger the length correction, or, in other words, the stronger the mistuning (Fig. 4). At a given frequency, the length correction increases roughly as the square of the curvature κ (Fig. 5).

Besides, the curves in Fig. 4 display particular behaviors that are almost independent of the curvature:

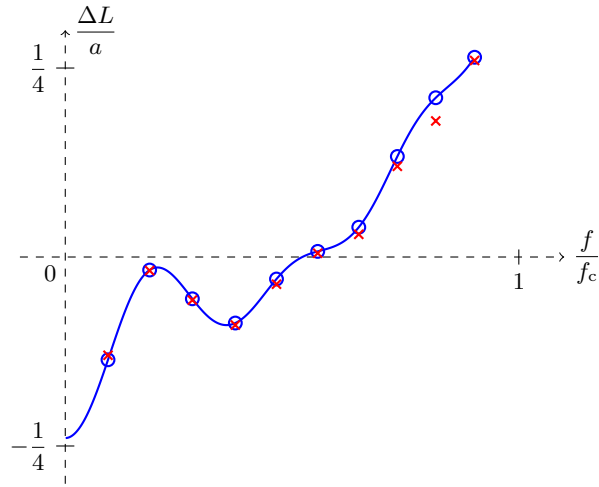
- A. the length correction passes through a minimum in absolute value - nearly zero - at the vicinity $f = 0.2f_c$,
- B. the sign of the length correction changes at a frequency close to $f_c/2$.

A. Minima of the length correction

Following the low frequency description made by Nederveen^{2,3} and Keefe and Benade⁴ (cf. Sec. II.B), one may expect the effect of curvature to vanish, or at least be lowered, when the position of the bend in a duct coincides with a node of the longitudinal velocity field. Indeed, if one supposes that the velocity node is located at the center of the bend in the



(a) Input impedance



(b) Length correction

FIG. 3. (a) Input impedance (modulus and phase) of the duct shown in Fig. 1, with $l_u/a = 3$, $l_b/a = 4\pi/3$, $l_d/a = 2$, and the "open" boundary condition $p = 0$ at the output end. The results, given for a curvature $\kappa = 0.5$ of the bend axis and computed with 12 modes taken into account (solid curve), are compared with the input impedance of a straight duct ($\kappa = 0$, dashed) with the same axis length L/a . (b) Length correction, in tube radius unit, for the same duct. Solid curve: length correction as defined by Eqs. (9-10), 'o': solutions of the dispersion relation (19) with a "closed" or "open" condition at the input end, 'x': finite differences method.

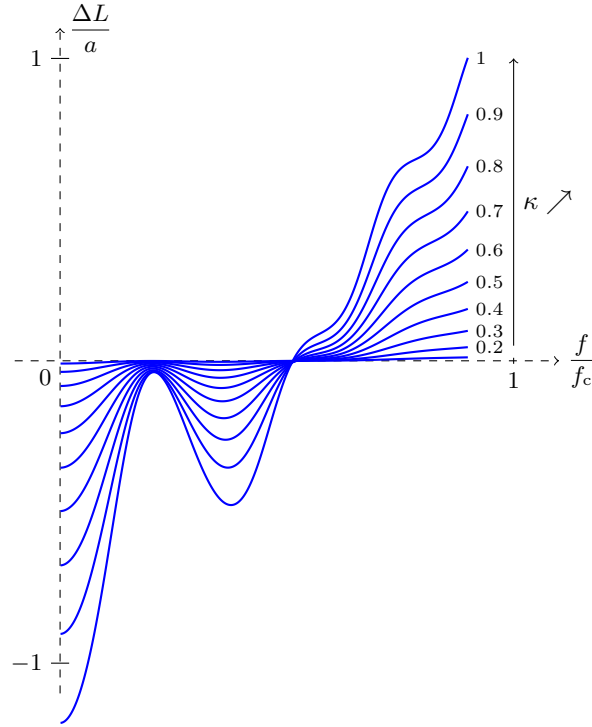


FIG. 4. Influence of the curvature on the length correction, as defined by Eqs. (9-10). The value of κ is increased from 0.1 (the curve, not labeled, is close the abscissa axis) to 1, in steps of 0.1.

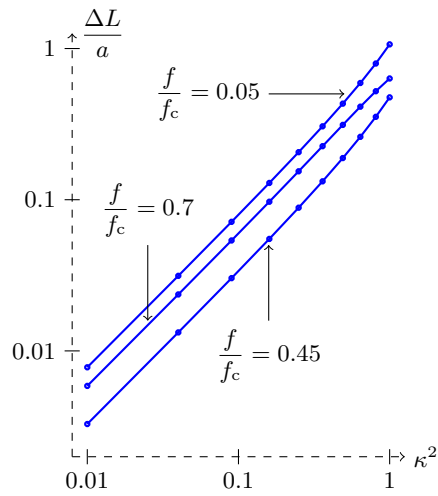


FIG. 5. Influence of the curvature on the length correction, as defined by Eqs. (9-10): ΔL increases as, roughly, the square of κ , at a given frequency.

example of Fig. 3, it follows that $\lambda/4 = l_b/2 + l_d$, where λ is the wavelength. Thus,

$$\frac{f}{f_c} = \frac{\pi a}{(l_b + 2l_d)\gamma_{10}} \simeq 0.2084. \quad (28)$$

If one varies the distance l_d from the output to the bend while keeping constant the curvature κ , the axis length of the bend l_b , and the overall length of the duct L , one observes a displacement of this local minimum of $|\Delta L|$ according to Eq. (28). The length correction does not exactly reach zero because at this frequency, the wavelength ($\lambda/a \simeq 16.4$) is not large compared with the length of the bend ($l_b/a \simeq 4.2$). Thus, the velocity field is not zero or negligible in the whole bend.

Besides, one can deduce that the length correction for a long duct with a bent portion will exhibit a large number of local minima (Fig. 6). In this case, the first minima appear at long wavelengths, compared with the bend size, therefore the length correction $|\Delta L|$ is close to zero at these frequencies.

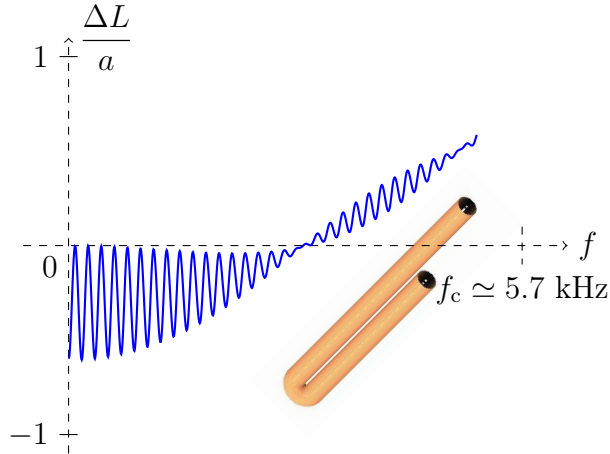


FIG. 6. Length correction, in tube radius unit, for a duct with $2a = 0.035 \text{ m}$, $\kappa = 0.78$, $l_u = 1.3 \text{ m}$, $l_b = \pi a/\kappa$, $l_d = 1 \text{ m}$ (the duct is somewhat similar to the air column of a contrabass clarinet), and an "ideal open end" condition $p = 0$ at the output end ($s = L$).

B. Frequency of the sign change

For frequencies below, and not too close to, the cutoff frequency f_c , the properties of the bent segment, notably the way the length correction varies with frequency, are mainly related to the characteristics of the first bend mode $\phi_0^{(\kappa)}$. As mentioned before (cf. Sec. II.C), it is possible to approximate this mode and its associated propagation constant $k_0^{(\kappa)}$, by computing the eigenmodes of the truncated matrix \mathcal{M} (Eq. 17). The propagation constant $k_0^{(\kappa)}$ is an increasing function of the frequency, that is lower than the propagation constant $k_0^{(0)} = k$ of the plane wave in a cylinder at low frequencies and higher near the cutoff (Fig. 7). A similar observation was made by Cummings¹⁸ in bends with rectangular cross-section, and borne out by El-Raheb.¹⁹ Therefore, if one assumes that the effect of the curvature at low frequencies is, roughly, to replace the plane wave propagating with a propagation constant $k_0^{(0)} = k$ by a quasi-plane wave propagating with the propagation constant $k_0^{(\kappa)}$, this explains qualitatively the variations of ΔL and the sign change.

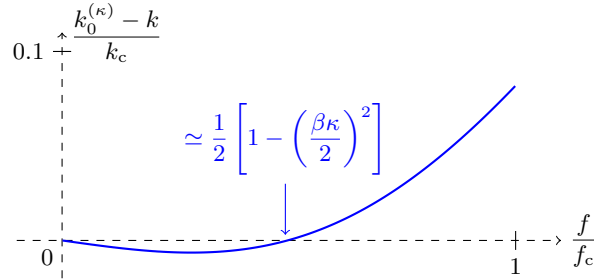


FIG. 7. Evolution with frequency of the propagation constant $k_0^{(\kappa)}$ of the first bend mode in a bend with curvature $\kappa = 0.5$, computed with 12 modes taken into account ($k_c = 2\pi f_c/c_0$).

If one takes into account only two modes in the multimodal formulation - the plane wave mode $\phi_0^{(0)}$ and the first evanescent mode $\phi_1^{(0)}$ - an approximation of $k_0^{(\kappa)}$ can be analytically calculated:

$$k_0^{(\kappa)} = \left[k^2(1 + \beta^2 \kappa^2) + \dots \right. \\ \left. \frac{1}{2} \left(\sqrt{k_c^4 - 8\beta^2 \kappa^2 k^2 (k_c^2 - 2k^2)} - k_c^2 \right) \right]^{1/2} \quad (29)$$

where

$$\beta = \frac{1}{\gamma_{10}^2 \sqrt{\frac{1}{2} \left(1 - \frac{1}{\gamma_{10}^2}\right)}} \simeq 0.5. \quad (30)$$

It differs from the “converged” value, computed with 12 modes (Fig. 7), by less than 0.3%.

The frequency at which $k_0^{(\kappa)} = k$ is

$$f_s = \frac{f_c}{2} \left[1 - \left(\frac{\beta \kappa}{2} \right)^2 \right]. \quad (31)$$

It is weakly dependent of the curvature: the relative shift from $k_c/2$ varies between 0 and $\sim 6\%$.

Of course, from this result, the rigorous calculation that would lead to the properties of the length correction itself is not straightforward, but this gives basic elements to better understand how a bend can modify the propagation and resonances in a duct.

Another remark can be made from the results on $k_0^{(\kappa)}$: the inertance correction (12) was first deduced by Nederveen² from a simplified formulation of the conservation equations in the long wavelength limit [Eq. (11)]. If, in a rough approximation, a low frequency wave in a bend is assumed to propagate with a propagation constant $k_0^{(\kappa)}$, then the coefficient α should be related to the zero frequency limit of $(k_0^{(\kappa)}/k)^2$. Indeed, the relative difference between α and this limit remains under 5% until $\kappa \simeq 0.96$ (Fig. 8).

IV. EXPERIMENTAL VERIFICATION OF THE FREQUENCY SHIFT DUE TO THE CURVATURE

To test the results, a duct was made in the workshop with a constant diameter $2a = 35$ mm and a toroidal bend with a κ of 7/9, somewhat similar to the bend in a contra-bass clarinet (Fig. 9). Its input impedance was measured using a set-up developed jointly by LAUM (Laboratory of Acoustics, Université du Maine, Le Mans, France) and CTTM (Center for Technology Transfer, Le Mans, France).²⁰ It consists in placing at the input

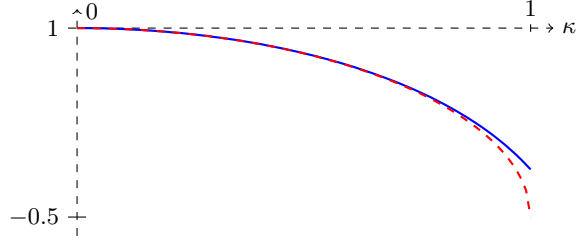


FIG. 8. Solid curve: zero frequency limit of $(k_0^{(\kappa)}/k)^2$, as approximated by its value at $f/f_c \simeq 5.10^{-6}$, computed with 12 modes taken into account, as a function of the curvature. Dashed curve: inertance correction α (Eq. 12).

of the measured instrument a piezo-electric source with a small closed cavity at its back. While a first microphone measures the pressure at the input of the instrument, a second microphone measures the pressure in the back cavity. Assuming the latter to be proportional to the volume velocity of the source, the input impedance of the measured object is then calculated from the transfer function between the two microphones, assuming that the motion of the piezo-electric transducer results in equal but out of phase volume velocity on both sides of the transducer. The reader may refer to Ref.²¹ for details on this set-up.

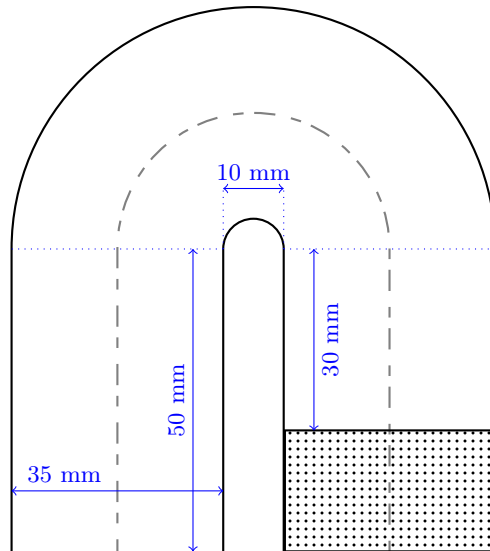
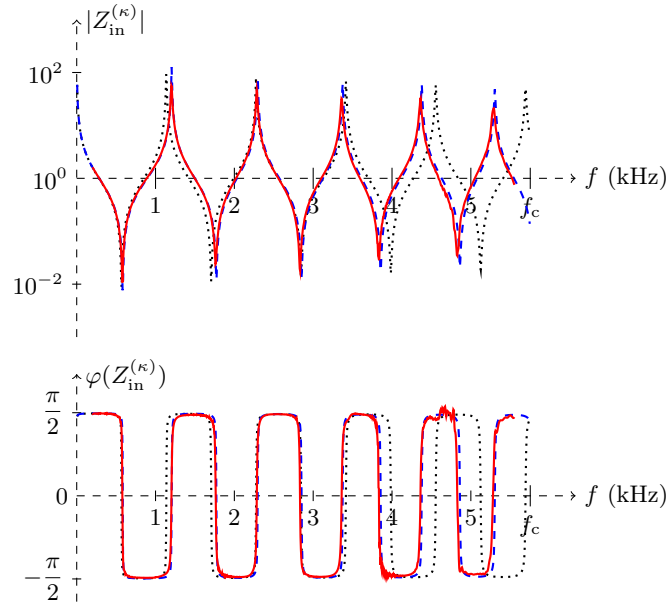


FIG. 9. Dimensions of the duct designed for the experiments. The axis curvature of the bend is $\kappa = 7/9$ and the duct is closed at the output.

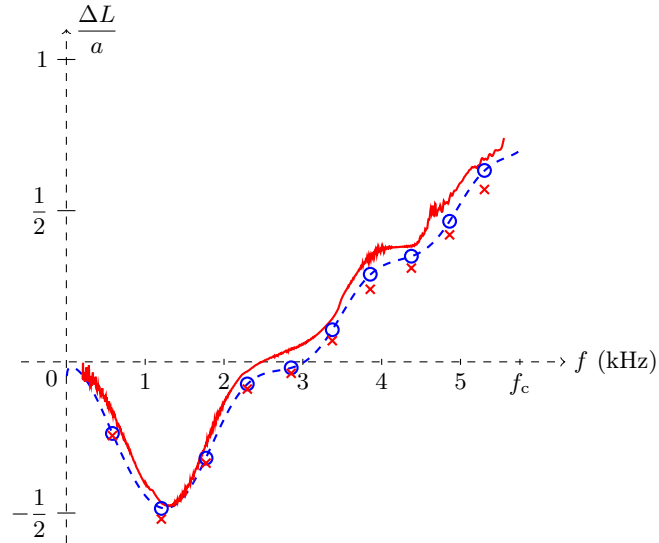
The frequency range of interest, from zero to the first cutoff $f_c \simeq 5.76$ kHz, is decomposed in four overlapping intervals, in order to maximize the signal-to-noise ratio (SNR) without saturation of the measured signal. For each interval, a 1 s long logarithmic chirp is used as input signal, leading to a frequency resolution of 1 Hz. The temperature in the tube is determined from a prior measurement of the input impedance of a closed cylindrical tube of known dimensions. For each tube, the acquisition is repeated five times and averaged. The calibration of the impedance sensor is described in the paper by Macaluso and Dalmont.²¹ The residual error is evaluated by calculating the difference between the measured input impedance of the straight tube with the theoretical value. Then the difference is used (except at its "singularities," that is, at the resonances of the straight tube) as a correction to the measured input impedance of the curved tube.

The measured input impedance is shown in Fig. 10(a). It is compared with the theoretical input impedance, computed as described earlier in the paper. To take into account the visco-thermal losses at the walls in the multimodal formulation, the purely real or purely imaginary propagation constants of the modes $\phi_n^{(0)}$ are replaced by complex propagation factors.^{13,22} Note, however, that this way of introducing the losses is not fully rigorous, since it assumes that the wall on which the boundary layer lies is locally plane. Therefore, the effect of the curvature of the boundary layer is not taken into account. Further investigations will be made on this particular aspect. In Eq. (9) the wavenumber k is replaced by a complex wave number, as classically done.²³

Fig. 10(b) shows the comparison of the measured length correction with the theoretical and numerical results from the multimodal and finite difference methods. The agreement is good over the whole frequency range. The shift of about 0.05 between the two curves can be explained by a possible temperature difference between the two measured tubes and the uncertainty in the temperature evaluation from the input impedance of the straight tube.



(a) Input impedance



(b) Length correction

FIG. 10. (a) Input impedance (modulus and phase) and (b) length correction for the duct shown in Fig. 9. Solid: experimental results. Dashed: theoretical results (the theoretical and experimental impedance curves are almost superimposed). Dotted: theoretical input impedance of a straight duct having the same radius and length. 'o': Solutions of Eq. (19) with a "closed" or "open" condition at the input end. 'x': Finite differences method.

V. CONCLUSION

The effects of bending a portion of a duct have been investigated theoretically and experimentally. Results show that the frequency shift induced by the curvature is not always small and, moreover, is strongly frequency dependent. It notably exhibits a sign change, so that the first resonance frequencies in a bent tube are shifted towards higher values, while they are shifted towards lower values near the cutoff. It has been shown that the magnitude of the frequency shift varies, roughly, as the square of the curvature, and that the frequency of the sign change is weakly dependent on the curvature. In this paper, only lossless or weakly lossy cases have been considered, with an approximate description of the visco-thermal losses at walls. Earlier studies have shown, however, the significant influence of the curvature on the wave propagation in a lined bend, notably the effect of localized wall losses⁸. Future studies of this matter should then involve a more comprehensive study of the lossy propagation in a bend.

Acknowledgments

The authors wish to thank Joël Gilbert for fruitful discussions.

References

- ¹ J. W. S. Rayleigh, *Theory of Sound*, volume 2, section 263 (McMillan and Company, London) (1878).
- ² C. J. Nederveen, *Acoustical aspects of woodwind instruments*, 2nd edition, pp. 60–62 (Northern Illinois University Press, Dekalb, IL) (1998).
- ³ C. J. Nederveen, “Influence of a toroidal bend on wind instrument tuning”, *J. Acoust. Soc. Am.* **104**, 1616–1626 (1998).
- ⁴ D. H. Keefe and A. H. Benade, “Wave propagation in strongly curved ducts”, *J. Acoust. Soc. Am.* **74**, 320–332 (1983).

- ⁵ G. S. Brindley, “Speed of sound in bent tubes and the design of wind instruments”, *Nature* **246**, 479–480 (1973).
- ⁶ J. W. Coltman, “Compensating for miter bends in cylindrical tubing”, *J. Acoust. Soc. Am.* **121**, 2497–2498 (2007).
- ⁷ S. Félix and V. Pagneux, “Multimodal analysis of acoustic propagation in three-dimensional bends”, *Wave Motion* **36**, 157–168 (2002).
- ⁸ S. Félix and V. Pagneux, “Sound attenuation in lined bends”, *J. Acoust. Soc. Am.* **116**, 1921–1931 (2004).
- ⁹ S. Félix and V. Pagneux, “Sound propagation in rigid bends: A multimodal approach”, *J. Acoust. Soc. Am.* **110**, 1329–1337 (2001).
- ¹⁰ S. Félix and V. Pagneux, “Ray-wave correspondence in bent waveguides”, *Wave Motion* **41**, 339–355 (2005).
- ¹¹ C. K. W. Tam, “A study of sound transmission in curved duct bends by the Galerkin method”, *J. Sound Vib.* **45**, 91–104 (1976).
- ¹² V. Pagneux, N. Amir, and J. Kergomard, “A study of wave propagation in varying cross-section waveguides by modal decomposition - part 1: Theory and validation”, *J. Acoust. Soc. Am.* **100**, 2034–2048 (1996).
- ¹³ N. Amir, V. Pagneux, and J. Kergomard, “A study of wave propagation in varying cross-section waveguides by modal decomposition - part II: Results”, *J. Acoust. Soc. Am.* **101**, 2504–2517 (1997).
- ¹⁴ S. V. Patankar, *Numerical heat transfer and fluid flow*, p. 59 (Taylor and Francis, London) (1980).
- ¹⁵ C. J. Nederveen and J.-P. Dalmont, “Corrections to the plane-wave approximation in rapidly flaring horns”, *Acta Acustica united with Acustica* **94**, 461–473 (2008).
- ¹⁶ D. Zwillinger, *Handbook of differential equations*, p. 579 (Academic Press, New York) (1992).
- ¹⁷ M. Abramowitz and I. A. Stegun, *Handbook of Mathematical Functions*, p. 883 (Dover, New York) (1970).

- ¹⁸ A. Cummings, “Sound transmission in curved duct bends”, *J. Sound Vib.* **35**, 451–477 (1974).
- ¹⁹ M. El-Raheb, “Acoustic propagation in rigid three-dimensional waveguides”, *J. Acoust. Soc. Am.* **67**, 1924–1930 (1980).
- ²⁰ J.-P. Dalmont and J.-C. Le Roux, “A new impedance sensor for wind instruments (A)”, *J. Acoust. Soc. Am.* **123**, 3014 (2008).
- ²¹ C. A. Macaluso and J.-P. Dalmont, “Trumpet with near-perfect harmonicity: Design and acoustic results”, *J. Acoust. Soc. Am.* **129**, 404–414 (2011).
- ²² A.-M. Bruneau, M. Bruneau, P. Herzog, and J. Kergomard, “Boundary layer attenuation of higher order modes in waveguides”, *J. Sound Vib.* **119**, 15–27 (1987).
- ²³ J.-P. Dalmont, K. Nederveen, and N. Joly, “Radiation impedance of tubes with different flanges: Numerical and experimental investigations”, *J. Sound Vib.* **244**, 505–534 (2011).

List of Figures

- FIG. 1 Duct with a bent portion. s is the abscissa along the waveguide axis, measured from the input of the duct (top), and $L = l_u + l_b + l_d$ is the total length of the duct axis. 4
- FIG. 2 Grid layout for the FDM solution in a bent segment connected to a straight segment. 12
- FIG. 3 (a) Input impedance (modulus and phase) of the duct shown in Fig. 1, with $l_u/a = 3$, $l_b/a = 4\pi/3$, $l_d/a = 2$, and the "open" boundary condition $p = 0$ at the output end. The results, given for a curvature $\kappa = 0.5$ of the bend axis and computed with 12 modes taken into account (solid curve), are compared with the input impedance of a straight duct ($\kappa = 0$, dashed) with the same axis length L/a . (b) Length correction, in tube radius unit, for the same duct. Solid curve: length correction as defined by Eqs. (9-10), 'o': solutions of the dispersion relation (19) with a "closed" or "open" condition at the input end, 'x': finite differences method. 16
- FIG. 4 Influence of the curvature on the length correction, as defined by Eqs. (9-10). The value of κ is increased from 0.1 (the curve, not labeled, is close the abscissa axis) to 1, in steps of 0.1. 17
- FIG. 5 Influence of the curvature on the length correction, as defined by Eqs. (9-10): ΔL increases as, roughly, the square of κ , at a given frequency. 17
- FIG. 6 Length correction, in tube radius unit, for a duct with $2a = 0.035$ m, $\kappa = 0.78$, $l_u = 1.3$ m, $l_b = \pi a/\kappa$, $l_d = 1$ m (the duct is somewhat similar to the air column of a contrabass clarinet), and an "ideal open end" condition $p = 0$ at the output end ($s = L$). 18
- FIG. 7 Evolution with frequency of the propagation constant $k_0^{(\kappa)}$ of the first bend mode in a bend with curvature $\kappa = 0.5$, computed with 12 modes taken into account ($k_c = 2\pi f_c/c_0$). 19

- FIG. 8 Solid curve: zero frequency limit of $(k_0^{(\kappa)}/k)^2$, as approximated by its value at $f/f_c \simeq 5.10^{-6}$, computed with 12 modes taken into account, as a function of the curvature. Dashed curve: inertance correction α (Eq. 12). 21
- FIG. 9 Dimensions of the duct designed for the experiments. The axis curvature of the bend is $\kappa = 7/9$ and the duct is closed at the output. 21
- FIG. 10 (a) Input impedance (modulus and phase) and (b) length correction for the duct shown in Fig. 9. Solid: experimental results. Dashed: theoretical results (the theoretical and experimental impedance curves are almost superimposed). Dotted: theoretical input impedance of a straight duct having the same radius and length. 'o': Solutions of Eq. (19) with a "closed" or "open" condition at the input end. 'x': Finite differences method. 23